Electric-field induced instabilities and morphological phase transitions in soft elastic films

Jayati Sarkar and Ashutosh Sharma*
Department of Chemical Engineering, Indian Institute of Technology Kanpur, UP 208 016, India

Vijay B. Shenoy†
Centre for Condensed Matter Theory and Department of Physics, Indian Institute of Science, Bangalore 560 012, India
(Received 17 December 2007; published 10 March 2008)

We investigate the morphological transitions of surface patterns induced in a soft elastic film in the presence of an applied electric field by the linear stability analysis and simulations. The surface patterns emerge beyond a critical strength of the electric field and the pattern length scale is always nearly three times the film thickness, regardless of the precise pattern morphology and other physical parameters. Interestingly, the simulations show that the precise pattern morphology depends strongly on the film and the field parameters and can be classified into three broad morphological phases: columns, stripes, and cavities. By tuning the electric field and the gap distance, we show that transitions from one morphological phase to another can be induced as described by a morphological phase diagram for this phenomenon. We also study the conditions under which the transitions can be "glassy" or "hysteretic." In addition to uncovering the rich physics underlying these nearly two-dimensional morphological phase transitions, our simulations also suggest experiments and applications of this phenomenon in mesopatterning. In particular, simulations demonstrate the possibility of controlling the pattern morphology and alignment by using the electric-field induced instability in soft elastic films. Unlike the short range adhesive interactions which cannot be varied, the use of an electric field allows far greater flexibility in modulation and control of the pattern morphology and its height.

DOI: 10.1103/PhysRevE.77.031604 PACS number(s): 68.15.+e, 89.75.Kd, 83.80.Va, 68.35.Np

I. INTRODUCTION

The physics of instabilities in soft liquid and solid thin films provides many scientifically interesting and technologically important issues [1–38]. The richness of the instability phenomena in soft films, both solid and liquid, arises from a competition between different types of energies such as the attractive-repulsive interfacial interactions, surface tension, and elastic stored energy. Understanding of surface phenomena in soft films and interfaces is important for many diverse problems such as peeling-debonding of adhesives, friction-cavitation-failure at soft interfaces, interactions between soft biological tissues, mesopatterning of soft materials, etc. [1–11].

In particular, electric-field induced self-organized structure formation in thin liquid films is already known to be a powerful potential method for mesopatterning of polymers [31–38]. We show here that electric field induced mesopatterning can also be achieved directly in soft solid elastic films, but the underlying physics that governs the structure length scale and morphology is quite distinct from that of a liquid film. Further, we show that the twin requirements of patterning, control of pattern morphology and order, can also be achieved by modulation of electric field applied to a thin solid film.

The basis of the electric-field induced pattern formation can be traced to the phenomenon of the elastic contact instability [12–15]. where the smooth surface of a soft solid thin film [made of a soft polymer, e.g., cross-linked polydimethyl siloxane (PDMS) or hydrogels] undergoes a spontaneous reorganization into a patterned state when it is in contact proximity of another surface. The most intriguing aspect of this instability is that the wavelength of the emergent pattern is usually about three times the film thickness and is essentially independent of all other factors such as the interfacial interactions and the mechanical properties. It is only for the submicron films that the surface tension also becomes important [16]. This elastic contact instability is now understood [20,21] to arise from a competition between the destabilizing attractive forces between the contacting surface and the film surface, such as the van der Waals and the electric field, and the stabilizing restoring elastic forces in the film. For a sinusoidal undulation of the film surface, the gain in the energy per unit area, because of the attractive interactions such as the van der Waals and electric field, is independent of the wavelength of the undulation [20,21], while the elastic energy cost for the incompressible film has a minimum when the wavelength of the undulation is about three times the film thickness. An intermediate wavelength is preferred because the elastic energy penalty increases both for very short and long wavelengths. Thus if the effective van der Waals interaction is larger than a critical value, the van der Waals force induces the surface undulation. The critical value of the interaction is reached when the distance between the contactor and the film surface is below a critical value which is usually very small, of the order of a few tens of nanometers at the most for the van der Waals interaction. Thus the pattern amplitude at the onset of instability is also very small because of the amplitude confinement by the contactor. Further, the van der Waals interaction is a material property and thus its magnitude cannot be modulated. We will refer to this mode of instability engendered by the short range van der Waals attractive force as the elastic contact

*ashutos@iitk.ac.in
†shenoy@physics.iisc.ernet.in

instability. The major objective of this study is to study the onset and control of the morphology of the elastic surface instability by application of an external electric field which can be easily modulated. Towards this end, we study the hallmarks of the instability when both the van der Waals and the electric field act together and also when the dominant influence is that of the electric field at larger gap distances. The earlier scenario is realistic for adhesion in air at short gap distances, whereas the latter case represents strong electric fields and also interactions across a liquid medium which matches nearly with the film in its van der Waals properties.

This elastic contact instability is quite distinct from the other known instabilities in soft films, particularly liquid films, where the emergent wavelength is a strong function of the interaction potential and the surface tension [22–24,31–38]. It has been shown that the contact instability of elastic films also plays an important role in the adhesion and peel-off behavior of soft films [25–29]. It was experimentally shown recently [30]. that the instability in elastic films can also be induced by an electric field which produces an effective attractive interaction between the film and contactor (electrode) surfaces, driven by the capacitive energy of the film-contactor system. As expected from theory [20,21]. the length scale of the emergent patterns was indeed found to be three times the film thickness, independent of the film properties and the applied potential, but the topology of the patterns was found to depend on the properties of the film.

The elastic contact instability has also been recently employed for mesoscale patterning applications in elastomers and hydrogels [16–19]. The short-range adhesive forces, such as the van der Waals, create instability at ~10 nm distance. Thus the height of the pattern formed is also confined by the contactor to a very small value. The height can be increased only by pulling the contactor away while still maintaining its parallel configuration with the film and the adhesion with the pattern. Moreover, the pattern morphology can be modulated only by increasing the stamp separation because the strength of van der Waals force cannot be changed [16–19]. We thus explore the possibility of controlling the instability and the pattern morphology by application of an external electric field, which can be applied at longer distances and can be modulated readily. As shown by the simulations here, such an approach of replacing the weaker and short-ranged adhesive forces by an electric field leads to a far greater flexibility in the control and modulation of the instability and in fabrication of high aspect ratio structures.

Motivated by the above issues, we present here a theoretical study of the patterns formed in a soft thin elastic film subjected to an external electric field. Our simulations address two important fundamental aspects of the problem, suggesting new experiments: (1) morphology of the electric-field induced patterns at the onset of instability, with focus on the role of the physical properties such as the thickness and shear modulus of the film in tuning the critical morphology, i.e., the morphology when the electric field is just large enough to induce an instability in the film, and (2) the subsequent *in situ* control of this morphology with tuning of the electric field. We show that several distinct critical morphologies can be engineered by tuning the properties of the film and that these morphologies can be modulated further by increasing the electric field. The third issue addressed is the use of a prepatterned electrode for the morphological control of the instability and resulting patterns. Simulations show that the isotropic instability patterns obtained using a flat electrode can be aligned and ordered by the use of a patterned electrode. This has direct implications for the use of elastic contact instability in mesopatterning of soft elastic films using an external electric field.

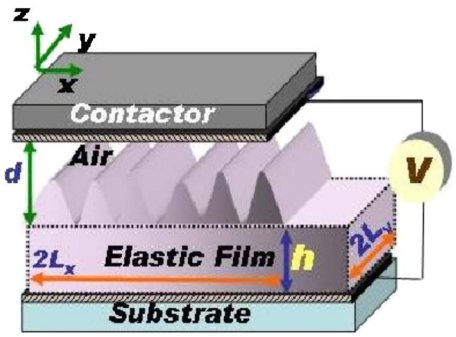

FIG. 1. (Color online) Schematic (not to scale) of film-contactor system with an air gap d and an applied voltage V. The film of thickness h is made of an incompressible elastic material of shear modulus μ and dielectric constant ε_f.

The paper is organized as follows. In Sec. II we present the theoretical formulation used for simulating the electric-field induced instability, including the analytical derivation of the critical field (voltage, see Fig. 1) necessary to induce the instability. Section III discusses simulation results for the patterns emergent at the critical voltage, followed by a discussion, in Sec. IV, of the evolution of the patterns with changing voltage. The possibility of using this instability to generate or transfer patterns from a prepatterned contactor is investigated by simulations in Sec. V. Summary of the results and conclusions are presented in Sec. VI.

II. THEORETICAL FORMULATION

The emergent patterns in the soft (nearly incompressible) elastic film (thickness h and shear modulus μ) on the application of electric field is due to a competition between the (destabilizing) capacitive electrostatic energy and the (stabilizing) elastic restoring forces. Figure 1 shows the system considered here consisting of an incompressible elastic film (thickness h, shear modulus μ) and a contactor with an enclosed air gap of thickness d, and with an applied voltage V across it. We develop a theoretical description of this model in terms of an energy function that contains both the elastic and electrostatic contributions to the total energy:

$$\Pi = \int_{\nu} d\nu\, W(\varepsilon_{ij}) + \int_{S} dS\, U(d - u_n), \tag{1}$$

where ν and S are, respectively, the volume and surface of the film, W is the strain energy density (ε_{ij} is the strain tensor), $U(u_n)$ is the electrostatic energy per unit area, given by

$$U(d-u_n) = -\frac{\varepsilon_0\varepsilon_f V^2}{2[(\varepsilon_f-1)(d-u_n)+d+h]} - \frac{A}{12\pi(d-u_n)^2} + \frac{B}{(d-u_n)^8}, \quad (2)$$

where V is the applied voltage, ε_f is the dielectric constant ($\approx$2.5 for PDMS films), ε_0 is the free-space permittivity (8.85×10^{-12} C^2/Jm), and u_n is the displacement of the film normal to the undeformed surface of the film. The second and third terms account for the interaction of the film with the contactor in the absence of electric field. This interaction term [16–19,25–29] consists of a van der Waals attractive part and a short-range Born repulsive part that arises from the overlap of the electronic orbits at very short distances. We consider two important cases to clearly differentiate the morphology of the van der Waals driven contact instability with the electric-field driven instability.

(1) There is an effective van der Waals attraction along with the short-range Born repulsion between the contactor and the film (in the absence of the applied electric field). The parameters chosen [16,20,25–27] to illustrate this behavior are $A=2.5\times10^{-20}$ J and $B=4.35\times10^{-82}$ J m^6 which correspond to an adhesive energy of 36 mJ/m^2. This case will be referred to as "films with the van der Waals attractive interaction."

(2) In order to assess separately the roles of van der Waals force and the electric field, we consider another limiting case where the van der Waals force is weak in comparison to the electric force or nearly switched-off. This may, for example, be achieved by introducing a liquid between the electrode and the contactor in the gap that has a Hamaker constant or van der Waals surface tension close to that of film or the electrode. For this case, we set $A=0$ and keep the same short-range Born repulsion as in the previous case. This case will be referred to as "films without the van der Waals interaction" in the text below. It is understood that the electric field and the very short-range Born repulsion, which prevents the contact singularity, are present in both cases.

The electrostatic energy promotes the deformation of the film surface, while the incompressible elastic nature of the film prefers homogeneous film morphology. A linear stability analysis [20,21,30] provides the condition for the emergence of inhomogeneous deformation morphology. In the present case, the condition for the emergence of inhomogeneous patterns is

$$-\frac{hY}{\mu} = \frac{h\varepsilon_0\varepsilon_f(\varepsilon_f-1)^2V^2}{\mu(h+\varepsilon_f d)^3} \geqslant 6.22, \quad (3)$$

where $Y=U''(d)$ is the "interaction stiffness." For a fixed d, Eq. (3) provides a critical voltage (V_c; for $d\ll h$, $V_c^2\sim\mu h^2$) for the onset of patterns; alternatively, for a given voltage V, Eq. (3) provides the critical gap distance d_c below which the film acquires a patterned morphology. The analysis predicts that the wavelength of the emergent pattern is of the order of three times the film thickness ($\lambda=3h$) at a critical strength of the applied force. While the critical force depends on the film properties, the resulting pattern length scale is independent of all properties except the film thickness. Note that this simple analysis for Y [Eq. (3)], neglects the short-range van der Waals and Born repulsion terms at the onset of instability induced by the electric field. This is justified since we are interested in cases where the gap distance d is larger than distance at which these surface adhesive interactions are strong enough. In realistic systems, the externally applied electric field is easily the dominant force at the gap distances $\geqslant$20 nm.

When the voltage exceeds the critical value given in Eq. (3), the film surface undergoes a morphological transition and assumes a patterned configuration. As will be shown here, the dominant length scale of this pattern is indeed always about $3h$ (three times film thickness) as shown by the linear stability arguments [20,21]. However, the precise morphology cannot be predicted by the linear stability analysis. When the voltage exceeds the critical voltage, the film surface morphology is determined by finding the normal displacement function $u_n(x,y)$ that minimizes the energy in Eq. (2). This nonlinear energy minimization process is achieved by expanding $u_n(x,y)$ in a Fourier series and casting Eq. (2) in terms of the Fourier coefficients. The Fourier coefficients that minimize the energy are determined using the conjugate gradient technique (see Ref. [16] for details) and these coefficients then determine the morphology. Unless otherwise stated, all the simulations reported in this paper are performed on the XY domains of size $32h\times32h$ (h is the film thickness) with 64^2 Fourier coefficients employing periodic boundary conditions.

The simulations reveal that the electric-field induced patterns that emerge in the films depend systematically on the physical parameters. We find that the emergent structures or morphologies can be classified into three basic types: (a) columns, (b) stripes, and (c) cavities. The columnar structure (see Fig. 2) consists of a film surface deformation in which a small fraction (less than half) of the film attains complete contact with the contactor. These areas of intimate contact are nearly circular. Interestingly, in some cases, the pillars are regularly spaced in a "triangular lattice," and yet in other cases, appear in an "amorphous" arrangement with some short-range order devoid of any long-range correlations.

The stripe morphology consists of long meandering channels of intimate contact that are equally spaced with roughly half of the film surface in contact with the electrode. These channels form "domains" in which they possess the same orientation and the domains are separated by domain boundaries. These structures are nearly bicontinuous at the transition between the pillar and cavity phases.

In the third morphology type, a larger fraction of the film surface is in intimate contact with the contactor and regions not in contact form regularly spaced cavities which, like the columns, can be placed in a nearly perfect triangular lattice. The key feature to be noted is that in all cases, the length scale (the spacing between columns, stripes, or cavities) is always about three times the film thickness as predicted by the linear stability analysis discussed above. Further, one type of structure can be morphed into another by controlling the voltage and other physical parameters of the system. We shall discuss first the emergent patterns at the critical voltage followed by the evolution of the patterns with the change of voltage.

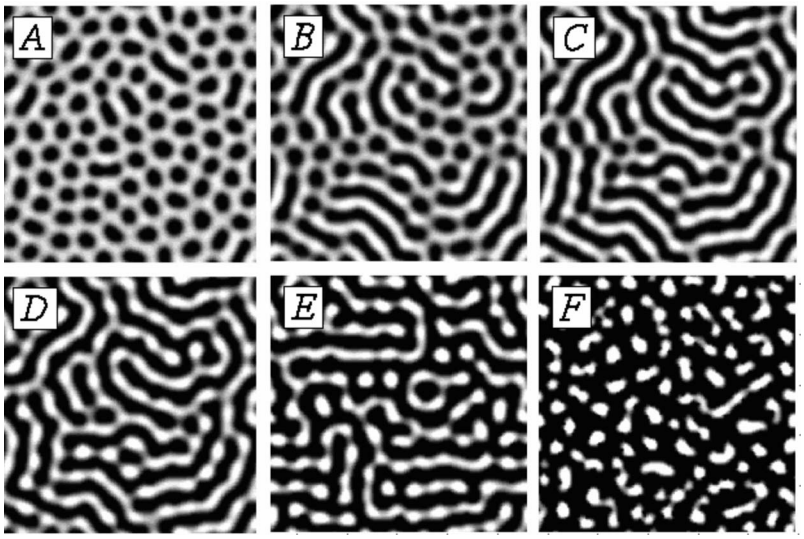

FIG. 2. Morphologies at critical voltage ($V=V_c$) in films ($\mu=0.1$ MPa and $h=1.0$ μm) with attractive van der Waals interaction with the contactor. The values of h/d for the figures are (A) $h/d=10$, (B) $h/d=30$, (C) $h/d=40$, (D) $h/d=50$, (E) $h/d=70$, and (F) $h/d=100$. The darkest areas in the figure correspond to regions where the film is in intimate contact with the contactor, and the brightest correspond to where the film is furthest away from the contactor. For small values of h/d ($h/d<20$, large air gap distances) the morphology consists of columns; for intermediate values h/d ($20\leqslant h/d\leqslant 70$), the morphology consists of stripes, while for larger values of h/d, cavities are obtained.

III. PATTERNS AT THE CRITICAL VOLTAGE

We first discuss the morphologies that emerge when the voltage is set to the critical voltage which depends on the film thickness h, the shear modulus μ, and the gap distance d via Eq. (3) (for $h=1$ μm, $\mu=0.1$ MPa, $d=100$ nm, and the critical $V_c=156$ V). Figure 2 shows the morphologies at the critical voltage for films that also have an attractive van der Waals interaction with the electrode. For a given gap distance and film thickness, the film morphology at the critical voltage is essentially independent of the shear modulus (in the experimentally relevant range 0.1–10.0 MPa). For a particular film thickness, the emergent morphology is columnar for larger gap distances, and with a decrease in the gap distance, the morphology changes to stripes and eventually to cavities. As is seen from Fig. 2, for $h/d<20$ the patterns at the critical voltage correspond to a columnar morphology, while for $20\leqslant h/d\leqslant 70$ a stripelike morphology is obtained, and finally, for $h/d>70$ a morphology with cavities is found. Interestingly, as shown in Fig. 3, very similar results concerning the basic pattern morphology are also obtained for films without the van der Waals interaction. This suggests that the key physics that determines the nature of the emergent pattern is the competition between the elastic energy and the electrostatic energy. Comparison of Figs. 2 and 3 also reveals that the short-range, rapidly decaying van der Walls interaction introduces a certain degree of disorder in the patterns, which are otherwise hexagonally ordered because of the electric field at both small and large values of the parameter, h/d (Fig. 3).

If the film surface attains complete contact with the electrode, the reduction of the electrostatic energy per unit area from the undisturbed state is given by

$$\Delta\Pi_{ES}=\frac{d(\varepsilon_f-1)\varepsilon_f\varepsilon_0V^2}{2(d+h)(h+\varepsilon_f d)}. \tag{4}$$

The elastic energy (per unit area) is proportional to $C\mu d^2/h$, where C is a dimensionless constant. At the critical voltage, the ratio R (energy ratio) of the reduction in the electrostatic energy to the increase in elastic energy (setting aside the constant C) is given by

$$R=\frac{3.11(d\varepsilon_f+h)^2}{d(\varepsilon_f-1)(d+h)}\sim\frac{h}{d}. \tag{5}$$

The morphology that develops is intimately related to the energy ratio R, which is proportional to h/d. This explains that the morphology at the critical voltage is insensitive to the shear modulus, as stated earlier. For large values of R, it is energetically favorable to have larger areas of the film in

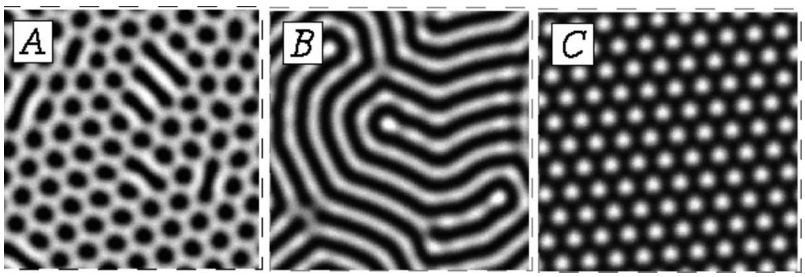

FIG. 3. Morphologies at critical voltage ($V=V_c$) in films ($\mu=1$ MPa and $h=1.0$ μm) without the van der Waals force. The values of h/d for the figures are (A) $h/d=15$, (B) $h/d=50$, and (C) $h/d=80$. The darkest areas in the figure correspond to regions where the film is in intimate contact with the contactor, and the brightest correspond to where the film is furthest away from the contactor. For small values of h/d ($h/d<20$, large air gap distances) the morphology consists of columns; for intermediate values of h/d ($20\leqslant h/d\leqslant 70$), the morphology consists of stripes, while for larger values of h/d, cavities are obtained. Compare with Fig. 2.

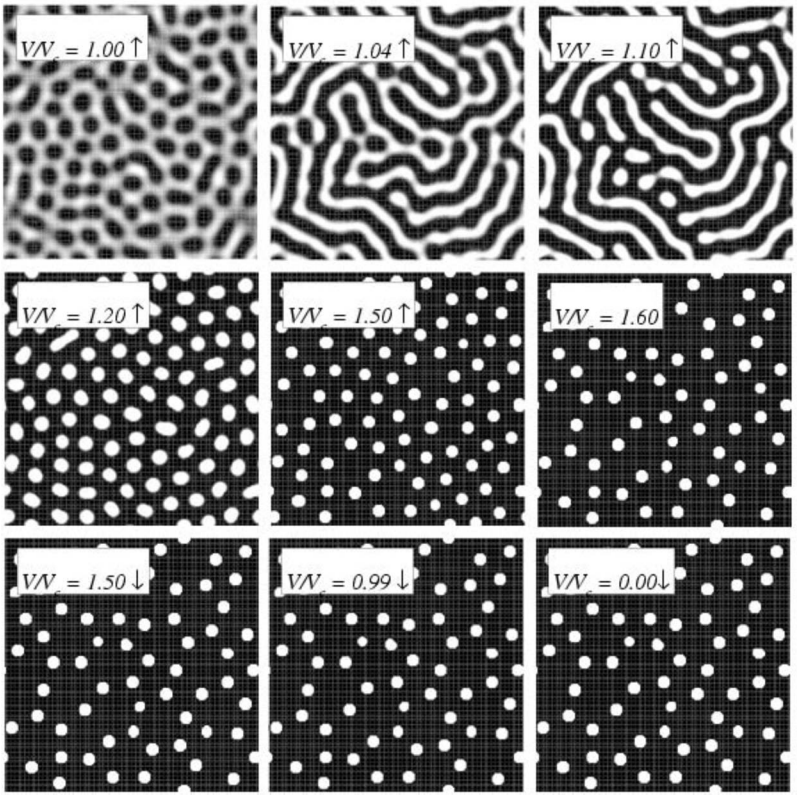

FIG. 4. Morphological evolution with applied voltage of patterns in films (μ=0.1 MPa and h =1.0 μm) with van der Waals attraction with an air gap d=50 nm. The critical voltage V_c =133 V. Starting from an arrangement of columns, the patterns evolve to stripes and cavities with increasing voltage V (indicated by an ↑ in the figure). The panels with the ↓ indicate the patterns when the voltage is reduced from the maximum applied voltage (V/V_c=1.6). Note that the patterns persist even to voltages below the critical voltage. See text for a discussion. The voltage changes are performed in steps of $\Delta V/V_c$=0.01.

intimate contact with the electrode, and a cavitylike morphology develops, while for small values of R the columnar morphologies are favored. In the intermediate range the favored configuration corresponds to stripe morphology where, roughly, half of the film surface is in intimate contact with the contactor.

It is interesting to view these results from the point of view of phase transitions. Considering the energy ratio R ($\equiv h/d$) as a parameter that is varied (with the voltage set to the critical voltage), it is clear that there exist two first order transitions: the first around R=20 where a columnar morphology transforms to the stripelike morphology, and the second around R=70 where the stripes give way to cavities. In the "column phase" the minimum energy configuration corresponds to a "triangular lattice" arrangement of the columns, while the equilibrium arrangement in the "stripe phase" is a pattern with parallel stripes. Similarly, in the "cavity phase" the equilibrium configuration is a "triangular lattice" arrangement of cavities. Note that the columnar or cavity phase completely breaks the translational symmetry of the energy function, while the stripe phase breaks translational symmetry only in one direction. Clearly the columnar phase and the cavity phases have the same symmetry but are "topologically inverted." Thus a transition from a columnar phase to a cavity phase is via a "topologically neutral" stripe phase (note that the "topologically inverted" phase of the stripe phase is again a stripe phase, and hence "neutral").

A comparison of the patterns obtained in the two cases (one with inclusion of the attractive van der Waals interaction and the second with only the electric field) shows that the morphologies are close to these equilibrium morphologies. In particular, in the case of weak van der Waals force (Fig. 3), it is evident that the equilibrium morphologies are very closely attained, although in each phase there are "domains," "grain boundaries" and "dislocations," i.e., topological defects. However, in the case with additional van der Waals attractive interaction between the film and the electrode (Fig. 2), the equilibrium is not attained nearly as well as it is in the case of the purely electric field. This is because of the many local minima in the energy landscape brought about by the presence of the attractive interactions; the system is trapped in such local minima and thus shows an increased "amorphous" character.

IV. VOLTAGE CONTROLLED EVOLUTION OF THE PATTERN

Next, we discuss the evolution of the patterns with increase of the voltage above the critical voltage. Figures 4 and 5 show the film morphologies when the applied voltage is above the critical voltage. Figure 4 includes the van der Waals attractive interaction and Fig. 5 is without the van der Waals interaction. With increasing voltage, the morphology evolves from columns to stripes and subsequently to an arrangement of cavities. The stripes form by the cooperative elongation of the circular contact regions of the columns. With further increase of voltage, the regions of the stripe structure not in contact with the electrode develop periodic contact zones and the final structure attained is an array of cavities.

Throughout the evolution process, the length scale (dominant wavelength) of the morphology still remains $3h$ as predicted by the linear stability theory at the onset of instability. In both cases (see Figs. 4 and 5), we have studied the evo-

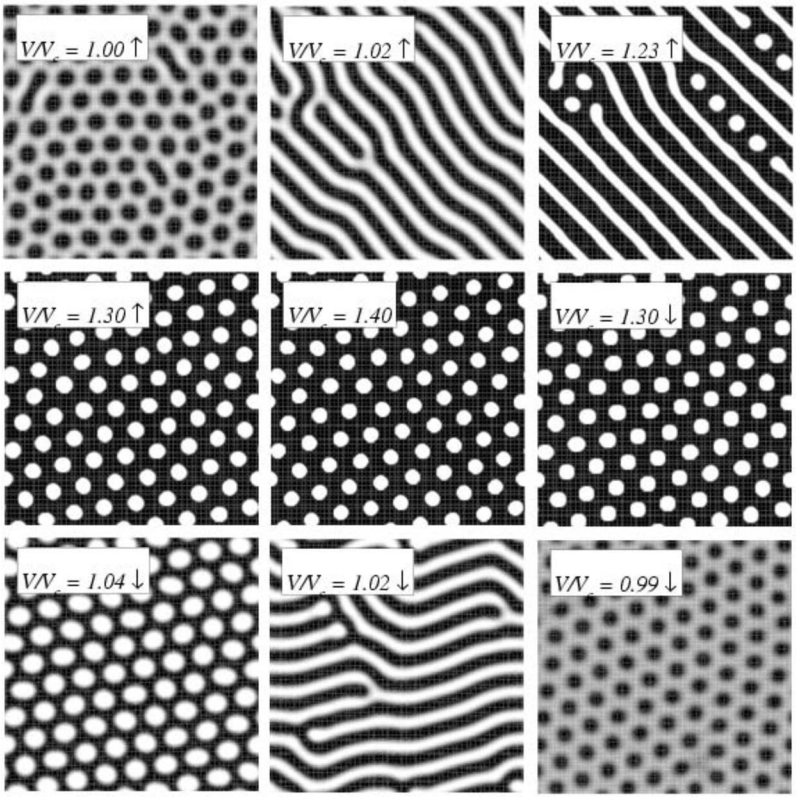

FIG. 5. Morphological evolution with applied voltage of patterns in films (μ=0.1 MPa and h =1.0 μm) without the van der Waals interaction and an air gap d=100 nm. The critical voltage V_c=156 V. Starting from an arrangement of columns, the patterns evolve to stripes and cavities with increasing voltage V (indicated by an ↑ in the figure). The panels with the ↓ indicate the patterns when the voltage is reduced from the maximum applied voltage (V/V_c=1.4). Note that the patterns disappear when the voltage is reduced below the critical voltage (not shown). See text for a discussion. The voltage changes are performed in steps of $\Delta V/V_c$=0.01.

lution of the patterns when the voltage is lowered back to zero in a gradual fashion from a predetermined maximum voltage. While the evolution of pattern is similar in the two cases during the ramping up of the voltage, the evolution is markedly different during the ramping down process as we discuss below.

First we discuss the case of a film with an attractive van der Waals interaction with the contactor. For such a film shown in Fig. 4, the morphology at the critical voltage is a set of pillars in a nearly "amorphous" arrangement. With the increase of voltage, the pattern evolves to a stripelike morphology, but in a rather gradual fashion, i.e., there is a "diffuse" first order transition, a transition that occurs gradually over many steps of the voltage. The stripes have "labyrinth" morphology; this is the "amorphous equivalent" of the stripe phase. Similarly, the transition from stripes to cavities is again a diffuse transition. On the appearance of cavities, which are, again, in an amorphous arrangement, further increase of voltage leads to interesting physics. The first effect is the decrease in the size of the cavities, followed by collapse of selected cavities leading to larger areas of intimate contact between the film and the contactor. Consequently, the length scale of the pattern at voltages well above the stripe-to-cavity transition voltage deviates markedly from the linear stability prediction. During the ramping down of the voltage, the evolution of the morphology is not reversed. Indeed, the wavelength of the pattern (spacing between cavities) remains frozen at the larger value attained at the maximum voltage and the cavities present at the maximum voltage grow reducing the total contact area.

Moreover, the pattern persists even when the voltage is reduced to well below the critical voltage, and the film attains its planar configuration only at a voltage which is less than half the critical voltage. For the films without the van der Waals attraction, the observations are quite different. As in the case of the attractive film, the initial morphology is a set of columns, which transform into stripes. However, the transition is rather abrupt and takes place over one or two steps of the voltage increment; i.e., it is closer to a true first order transition. At higher voltages, there is a transition to a set of cavities via "break up" of the stripes (see Fig. 5). This transition is again much sharper than in the case of films with an attractive interaction with the contactor. After the attainment of the cavity phase, further increase of voltage does not lead to significant increase of contact area and the cavities continue to maintain their near triangular lattice arrangement, again in contrast with the van der Waals film. During the ramping down of the voltage, the cavity phase is "supercooled," and the transition to the stripe phase occurs at a lower voltage along with a small range of voltage where the two phases coexist. The transition from the stripe phase to the column phase is completely reversible. Interestingly, the patterns completely disappear when the voltage is reduced below the critical value during the ramping down process, in stark contrast to the case of the film with an attractive interaction with the contactor. Thus in the case of van der Waals force, the pattern, once formed by the electric field, is "pinned" by the action of van der Waals attractive force.

The differences in the two cases, namely the films with an additional attractive interaction and the films without it, can be understood in terms of the energy landscape. As is known previously [25,26] and as noted above, the presence of the attractive interaction with the contactor results in the presence of deep local minima in the energy landscape. Once the

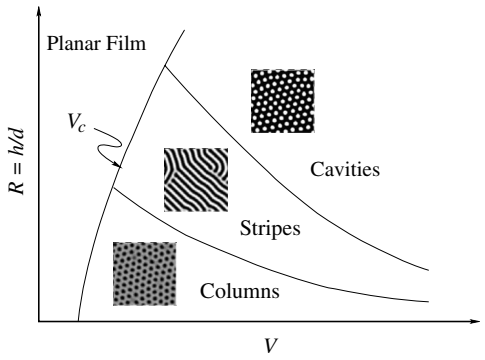

FIG. 6. Schematic morphological phase diagram of the film-contactor system in an electric field. See Fig. 1 for notation. In the case of films with attractive interaction with the contactor, the phases attained are "amorphous" equivalents of equilibrium phases shown here with diffuse-hysteretic transitions between them.

conditions favorable for the pattern formation are met (voltage above a critical value), the system settles down to the "nearest" minimum. The pattern attained is a metastable amorphous columnar state. Although further increase of voltage favors the stripe phase, the system is trapped in this local metastable minimum and transforms to the stripe phase over a range of voltage with a gradual coalescence of the columns to form stripes. Thus the presence of many local energy minima corresponding to different morphologies renders the transition a diffuse first order transition. Moreover, the stripe phase is itself in a metastable minimum as is seen by the "labyrinth" character of the stripes (many short and curved interpenetrating fingers like morphology). Similar physics applies to the transition between the stripe phase and the cavity phase, and the nature of the cavity phase is also amorphous. The increase of contact area is due to a large gain in the nonelectrostatic adhesive energy (because of the attractive interactions other than the electric field). This may be contrasted with the case of the film without the nonelectrostatic interactions, where there is no significant increase of the contact area in the cavity phase with increasing voltage. Without attractive interactions, the configuration attained deep in the cavity phase regime corresponds to a very deep metastable minimum and the system is trapped in this phase during the ramping down process. Moreover, as noted above in the case of attractive interaction, the patterns persist even at voltages lower than the critical voltage. The physics of this phenomenon is very similar to that of "adhesion-debonding hysteresis" noted in Refs. [25,26]; the reduction of the voltage in the present case is equivalent to the withdrawal of the contactor discussed in that paper. Interestingly, for films with larger shear modulus, this hysteresis can be largely suppressed; indeed, in simulations with attractive films with $\mu = 1$ MPa (all other parameters the same as shown in Fig. 4), we do not see the persistence of the patterns much below the critical voltage; this is again consistent with the findings of Refs. [25,26].

The results of the simulations presented here are summarized in a simple morphological phase diagram shown in Fig. 6. In the presence of a nonelectrostatic attractive interaction between the film and the contactor, the "amorphous equivalents" of equilibrium phases noted in the diagram are the ones that are attained with diffuse transitions between them. This phase diagram also suggests possible application of this phenomenon to patterning of soft films, while providing fundamental insights into this electric-field induced instability.

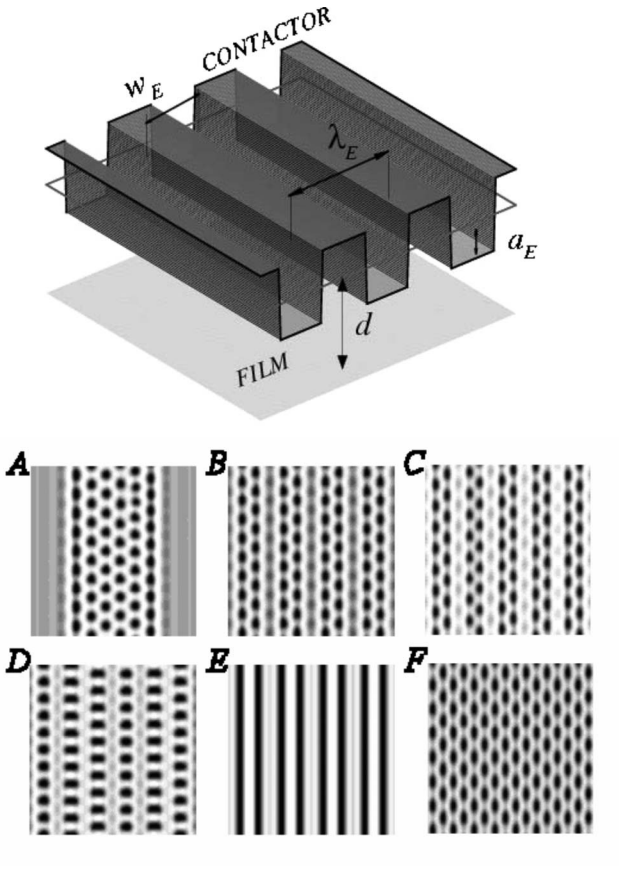

FIG. 7. Top: A step corrugated electrode used in patterning simulations. The width of the step is half the spacing between the steps (i.e., $w_E = \lambda_E/2$). The simulations are on films without van der Waals attraction with $\mu = 0.1$ MPa and $h = 3.8$ μm. The nominal gap distance $d = 210$ nm, the "amplitude" of the step $a_E = 10$ nm. The applied voltage is 512 V, which corresponds to the critical voltage for a gap distance of 200 nm. Bottom: (A) $\lambda_E = 32h$: triangular lattice pattern near the center of the step is terminated by a set of aligned columns near the edge of the step. (B) and (C) Two sets of aligned columns under each step for $\lambda_E = 32h/4$ and $\lambda_E = 32h/5$. (D) A set of single columns under each step for $\lambda_E = 32h/6$. (E) "Resonance patterning:" transfer of the contactor pattern for $\lambda_E = 32h/8$. (F) "Anisotropic triangular lattice" arrangement of columns for $\lambda_E = 32h/16$.

V. PATTERNING OF SOFT FILMS USING ELECTRIC FIELDS

In this section we explore the possibility of using the electric-field induced instabilities to pattern soft films. The key idea behind this approach is to induce spatially nonuniform electric fields via a prepatterned contactor electrode.

We first consider a step corrugated contactor electrode (see top panel of Fig. 7). The spacing between steps is λ_E,

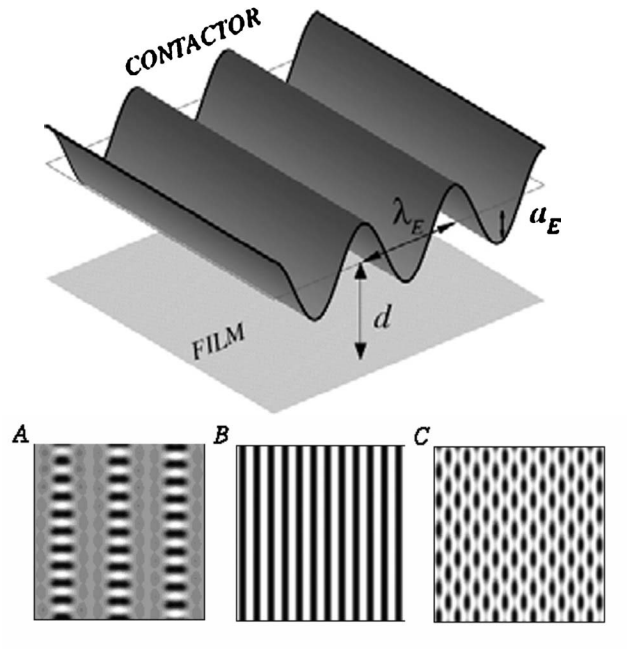

FIG. 8. Top: Sinusoidally patterned electrode. Bottom: (A) Single set of aligned columns for $\lambda_E=32h/3=10.67h$; (B) "resonance patterning" for $\lambda_E=32h/12=2.67h$; and (C) "anisotropic triangular lattice" for $\lambda_E=32h/18=1.78h$. The physical properties of the film and the applied voltage are the same as in Fig. 7.

while the width of the steps w_E is taken to be half the spacing, i.e., $w_E=\lambda_E/2$. The height of the steps is denoted by a_E, and the nominal gap distance between the film and electrode is denoted by d. The applied voltage is chosen to be the critical voltage for the minimum gap thickness, $(d\text{-}a_E)$ corresponding to the step faces closest to the film surface. All the relevant parameters chosen for this study are given in the caption of Fig. 7. We study here the nature of patterns that emerge when the spacing of the steps λ_E is varied. When the spacing of the steps and their width are large compared to the thickness of the film, the emergent pattern is set of columns arranged in a triangular lattice terminated by regularly spaced linear arrays of columns near the edges of the step [see Fig. 7(a)]. This simulation shows that electric-field induced patterning can be used to generate patterns over a finite area of the film. On reduction of the step spacing, the pattern obtained is a set of linear arrays of columns corresponding to the position of the steps [Figs. 7(b) and 7(c)]. The number of column arrays formed under each step is determined by the width (half the spacing in the present case). For a spacing of $32h/6$, we obtain an equispaced linear array of columns [Fig. 7(d)]. Interestingly, in all the cases discussed so far, spacing of the column in each linear array is $3h$.

When the spacing of the steps is about $3h$ (the characteristic scale in the system), the emergent pattern perfectly reproduces the electrode morphology—we refer to this phenomenon as "resonance patterning" [Fig. 7(e)]. Further decrease of step spacing produces an "anisotropic" triangular lattice of columns. We have also conducted similar studies with a sinusoidally patterned electrode (Fig. 8, top panel). The qualitative features of the patterns obtained in this case

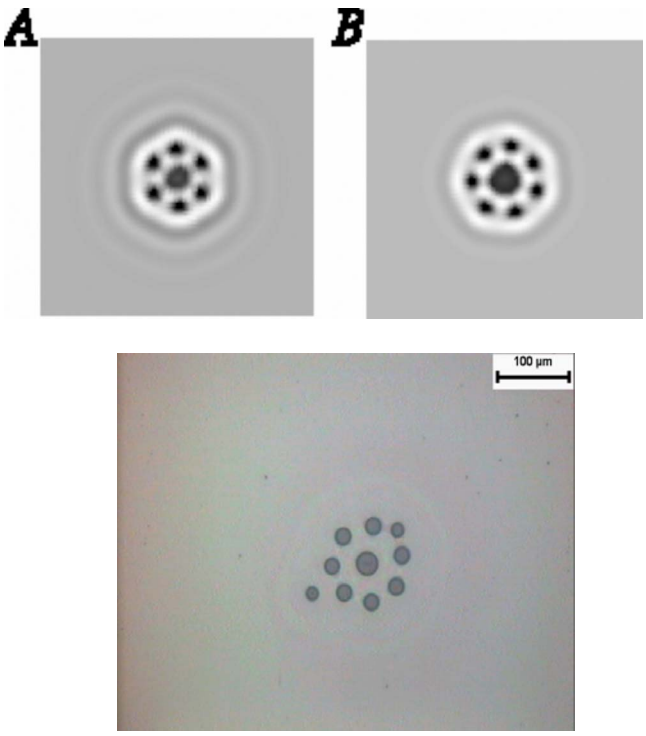

FIG. 9. (Color online) Simulations of patterns near a local heterogeneity in films with $\mu=0.1$ MPa and $h=3.8$ μm. The heterogeneity in this case is treated as a conical protrusion on the electrode with a height h_D and radius r_D. (A) Hexagonal arrangement of a set of six columns around a central column, the height of the dirt particle (h_D) is 0.1 μm, radius (r_D) is 12.16 μm. (B) A set of seven columns around a central column form for the same parameters as in (A) but with $r_D=13.68$ μm. (Bottom) A typical experimental observation of column formation on the surface of a cross-linked PDMS film around a defect. For this experiment, film thickness is ~ 9.0 μm, and wavelength intercolumn spacing is $\sim$ 38 μm, which is about $\sim 4h$.

are similar to those with the step corrugated electrode (Fig. 8 bottom panel). An earlier study [27] of the near contact instability engendered by the van der Waals interaction without the electric field also showed some rudimentary ordering of the structure. However, as shown here, application of a long-range electric field produces a far more regular pattern with smoother morphological features. This is because a much steeper decay of the van der Waals force compared to the electrostatic interaction results in a complex energy landscape with multiple energy minima. Thus from the point of view of mesopatterning, electric-field induced structuring appears to be a more promising technique.

In fact, a local ordering of elastic instability patterns was found to be quite ubiquitous in experiments, where the presence of a few dirt particles on the electrode creates locally inhomogeneous fields. Inspired by our laboratory observations of patterns that emerge in an elastic film near a dirt particle, we carried out simulations of patterns near a local heterogeneity of the electrode. Results are summarized in Fig. 9 where a local protrusion of the electrode is modeled as a conical protrusion of height h_D and radius r_D. The dirt particle is considered to be made of a large dielectric con-

stant. The electric field strength is highest over the cone area as compared to the other part of the film because of the reduced air gap which results in local patterning. The results of the simulations with dirt particles of two different radii are shown in Fig. 9. The key feature obtained from the simulations is a central column at the location of the conical protrusion surrounded by a set of satellite columns. The number of columns increases with the radius of the particle. Interestingly, the number of satellite columns is such that their circumferential spacing around the central column is again roughly $3h$. An experimental observation of such satellite column formation is also shown at the bottom of Fig. 9. Thus it can be concluded that spatially inhomogeneous electric fields can be used to produce locally ordered patterns in soft elastic films.

VI. CONCLUSION

In this paper, we have theoretically studied the morphology of the surface instability induced by an external electric field in a soft elastic thin film. The instability is due to a competition between the destabilizing electrostatic energy and the stabilizing elastic energy. The onset of instability occurs at a critical voltage when the stiffness of the applied electric force exceeds the elastic stiffness of the film. While the wavelength of the emergent critical pattern is determined only by the film thickness, the morphology of the pattern depends strongly on the ratio h/d. We have identified three basic types of pattern morphologies—columns, stripes, and cavities and also the conditions for their transition by varying the electric field. These may be considered as "surface phases" of the film, and it is possible to achieve "phase transitions" by tuning, for example, the voltage. A morphological phase diagram for this phenomenon is constructed from our simulations. An important finding is that in the case of films with an additional nonelectrostatic attractive interaction with the electrode, the system shows "glassiness" and the phase transitions become diffuse. It must be noted that the physics underlying the phenomenon we discuss here is qualitatively different from that of electric-field induced instabilities in liquid films [31–38].

These findings also have the potential to contribute to many technological applications. A key advantage of using the electric-field induced instability is that a long-range nature of the electric fields allows for a larger gap distance leading to better control of the processes involved. We have demonstrated via simulations that this phenomenon can lead to a robust method for mesopatterning of soft solid elastic films which includes the strategies for the control of pattern morphology and its order.

ACKNOWLEDGMENTS

A.S. acknowledges the support of the DST Unit on Nanoscience at IIT Kanpur. V.B.S. thanks DST for generous support.

[1] Y. Y. Lin, C.-Y. Hui, and H. D. Conway, J. Polym. Sci., Part B: Polym. Phys. **38**, 2769 (2000).
[2] C. Creton, J. Hooker, and K. R. Shull, Langmuir **17**, 4948 (2001).
[3] J. Crosby, K. R. Shull, H. Lakrout, and C. Creton, J. Appl. Phys. **88**, 2956 (2000).
[4] K. T. Wan, J. Adhes. **75**, 369 (2001).
[5] N. Gent and R. P. Petrich, Proc. R. Soc. London, Ser. A **310**, 433 (1969).
[6] I. Chikina and C. Gay, Phys. Rev. Lett. **85**, 4546 (2000).
[7] K. Brown, J. C. Hooker, and C. Creton, Macromol. Mater. Eng. **287**, 163 (2002).
[8] J. F. McCabe, T. E. Carrick, and H. Kamohara, Biomaterials **23**, 1347 (2002).
[9] D. A. Hammer and M. Tirrell, Annu. Rev. Mater. Sci. **26**, 651 (1996).
[10] S. K. Sia and G. M. Whitesides, Electrophoresis **24**, 3563 (2003).
[11] Y. Xia and G. M. Whitesides, Annu. Rev. Mater. Sci. **28**, 153 (1993).
[12] A. Ghatak, M. K. Chaudhury, V. B. Shenoy, and A. Sharma, Phys. Rev. Lett. **85**, 4329 (2000).
[13] K. R. Shull, C. M. Flanigan, and A. J. Crosby, Phys. Rev. Lett. **84**, 3057 (2000).
[14] W. Mönch and S. Herminghaus, Europhys. Lett. **53**, 525 (2001).
[15] A. Ghatak and M. K. Chaudhury, Langmuir **19**, 2621 (2003).
[16] M. Gonuguntla, A. Sharma, J. Sarkar, S. A. Subramanian, M. Ghosh, and V. Shenoy, Phys. Rev. Lett. **97**, 018303 (2006).
[17] M. Gonuguntla, A. Sharma, R. Mukherjee, and S. A. Subramanian, Langmuir **22**, 7066 (2006).
[18] M. Gonuguntla, A. Sharma, and S. A. Subramanian, Macromolecules **39**, 3365 (2006).
[19] A. Sharma, M. Gonuguntla, R. Mukherjee, S. A. Subramanian, and R. K. Pangule, J. Nanosci. Nanotechnol. **7**, 1744 (2007).
[20] V. Shenoy and A. Sharma, Phys. Rev. Lett. **86**, 119 (2001).
[21] V. Shenoy and A. Sharma, J. Mech. Phys. Solids **50**, 1155 (2002).
[22] S. Herminghaus, K. Jacobs, K. Mecke, J. Bischof, A. Fery, M. Ibn-Elhaj, and S. Schlagowski, Science **282**, 916 (1998).
[23] A. Sharma and R. Khanna, Phys. Rev. Lett. **81**, 3463 (1998).
[24] G. Reiter, R. Khanna, and A. Sharma, Phys. Rev. Lett. **85**, 1432 (2000).
[25] J. Sarkar, V. Shenoy, and A. Sharma, Phys. Rev. Lett. **93**, 018302 (2004).
[26] J. Sarkar, A. Sharma, and V. B. Shenoy, Langmuir **21**, 1457 (2005).
[27] J. Sarkar, A. Sharma, and V. Shenoy, J. Adhes. **81**, 1 (2005).
[28] A. Ghatak, Phys. Rev. E **73**, 041601 (2006).
[29] A. Ghatak, L. Mahadevan, M. K. Chaudhury, and V. Shenoy, Proc. R. Soc. London, Ser. A **460**, 2725 (2004).
[30] N. Arun, A. Sharma, V. Shenoy, and K. S. Narayan, Adv. Mater. (Weinheim, Ger.) **18**, 660 (2006).
[31] E. Schäffer, T. Thurn-Albrecht, T. P. Russell, and U. Steiner,

Nature (London) **403**, 874 (2000).
[32] E. Schäffer, T. Thurn-Albrecht, T. P. Russell, and U. Steiner, Europhys. Lett. **53**, 518 (2001).
[33] N. E. Voicu, S. Harkema, and U. Steiner, Adv. Funct. Mater. **16**, 926 (2006).
[34] S. Harkema and U. Steiner, Adv. Funct. Mater. **15**, 2016 (2005).
[35] M. D. Morariu, N. E. Voicu, E. Schäffer, Z. Lin, T. P. Russell, and U. Steiner, Nat. Mater. **2**, 48 (2003).
[36] N. E. Voicu, M. S. M. Saifullah, K. R. V. Subramanian, M. E. Wellandb, and U. Steiner, Soft Mater. **3**, 554 (2007).
[37] G. Tomar, V. Shankar, A. Sharma, and G. Biswas, J. Non-Newtonian Fluid Mech. **43**, 120 (2007).
[38] R. Verma, A. Sharma, K. Kargupta, and J. Bhaumik, Langmuir **21**, 3710 (2005).